Journal of Nonlinear Modeling and Analysis
Volume 8, Number 2, April 2026, 368–382
https://global-sci.com/jnma
DOI:10.12150/jnma.2026.368

Nonlinear Dynamics and Chaos in Fractional-Order Cardiac Action Potential Duration Mapping Model

Rabah Bououden[1], Tarek Houmor[2], Fahd Jarad[3,4,†] and Mohammed S. Abdelouahab[1]

Received 30 January 2025; Accepted 27 October 2025

Abstract This study introduces a novel one-dimensional fractional-order model for cardiac action potential duration (APD) dynamics, incorporating memory effects through discrete fractional calculus. By generalizing the classical APD map using the Caputo fractional difference operator, we uncover complex nonlinear behaviors not observed in traditional integer-order models. Through comprehensive numerical simulations, including bifurcation analysis and Lyapunov exponent calculations validated by the 0-1 test, we demonstrate that the fractional-order system exhibits:
1) Early onset of chaos (at $t_s = 307ms$) without preceding period-doubling bifurcations.
2) Novel rhythm alternations between $5:5$ and $3:3$ patterns.
3) Unique bistability phenomena, including $2:2 \longleftrightarrow chaos$ and $5:5 \longleftrightarrow 3:3$ states.
4) Memory-dependent dynamics where current APD depends on all previous states.
Our results reveal that fractional calculus provides a more physiologically realistic framework for modeling cardiac dynamics by naturally incorporating memory effects. The identified dynamical regimes offer new insights into the transition mechanisms from normal rhythms to potentially arrhythmic states, with particular clinical relevance to understanding alternans as precursors to ventricular fibrillation. The fractional-order approach demonstrates superior capability for capturing the complex, history-dependent nature of cardiac excitation compared with conventional models.

Keywords Fractional-order calculus, cardiac dynamics, action potential duration, nonlinear dynamics, chaos

MSC(2010) 34C28, 34C23.

[†]the corresponding author.
Email address: r.bouden@centre-univ-mila.dz(R. Bououden), tarek_houmor@umc.edu.dz(T. Houmor), fahd@cankaya.edu.tr(F. Jarad), m.abdelouahab@centre-univ-mila.dz(M. S. Abdelouahab)
[1]Laboratory of Mathematics and their Interactions, Abdelhafid Boussouf University, Mila 43000, Algeria.
[2]Applied Mathematics and Modeling Laboratory, Constantine 1-Mentouri University, Constantine 25017, Algeria.
[3]Department of Mathematics, Çankaya University, Etimesgut 06790, Ankara, Türkiye.
[4]Department of Engineering Mathematics and Artificial Intelligence, Azerbaijan Technical University, Hüseyn Cavid Av., Baku 1073, Azerbaijan.

1. Introduction

To understand cardiac arrhythmias in the human heart, it is essential to grasp the complex dynamics represented in mathematical models. The idea that mathematical analysis can aid in understanding these arrhythmias is not a recent development. As early as the 1920s, researchers showed that by adjusting parameters in mathematical models of the heart, they could replicate rhythms that are clinically observed in arrhythmias [12, 24].

The behavior of various cardiac arrhythmias and the transitions between different heart rhythms suggest that nonlinear phenomena play a significant role in the development of these irregular heartbeats. Unlike most cardiac diseases, which progress slowly and steadily over many years, arrhythmias can often occur suddenly. In nonlinear systems, sudden changes in dynamics can unexpectedly arise from gradual modifications to a system parameter; this phenomenon is known as bifurcation [20].

Memory has been the subject of extensive research across multiple disciplines, including physics, chemistry, biology and electrical engineering [1, 4, 17]. In systems characterized by memory, dynamic behavior is significantly influenced by prior experiences, as exemplified by hysteresis observed in ferromagnetic materials. In electrically excitable cells, such as neurons and cardiomyocytes, the dynamics of excitation are governed by intricate networks that encompass a variety of ion channels and signaling pathways, each functioning on distinct time scales. Consequently, these systems frequently exhibit memory effects. For instance, electrical bursting in neurons and pancreatic β-cells arises from interactions between rapid and slow time scales, with the slower time scales potentially contributing to the development of memory.

Low-dimensional iterated maps have been extensively employed to elucidate the dynamic mechanisms underlying complex cardiac excitations. One of the most widely recognized iterated map models is grounded in cardiac myocytes' action potential (AP) duration-restitution characteristics [26]. The concept of action potential duration (APD) restitution is well-established in cardiology and has undergone thorough investigation in various experimental studies [14, 27, 29]. These iterated maps demonstrate effectiveness when the influence of memory is negligible. However, their limitations become apparent when substantial memory effects indicate the need for higher-dimensional maps to capture these dynamics accurately. Previous research has examined the relationship between memory and cardiac alternans, generally concluding that memory exerts a suppressive effect on alternans [15,33,34].

Incorporating the memory effect into a model can be effectively achieved through the use of a fractional-order operator. Over the past four decades, fractional calculus—an extension of continuous-time and discrete-time chaotic dynamical systems to non-integer orders—has garnered significant attention [6–8, 18, 35]. This fascination is largely because fractional-order models provide a more precise representation of complex phenomena and reveal behaviors that integer-order models often overlook. Moreover, fractional calculus naturally aligns with systems characterized by memory, which are frequently found in numerous biological processes [2, 11, 19, 28, 30–32]. Embracing these models could lead to breakthroughs in understanding and analyzing intricate systems.

In this work, we will summarize the contributions made by Lewis and Guevara [23]. To incorporate the memory effect into their proposed model, we introduce a

fractional version of the model by utilizing the Caputo fractional order differential operator.

While traditional approaches to modeling cardiac electrical activity have provided valuable insights, they often fail to capture a critical feature of cardiac tissue (memory effects). Our discrete fractional order model provides an elegant framework to bridge this gap through its mathematical advantages and biological relevance, since it naturally incorporates memory through its non-local kernel, preserving the simplicity of 1D maps while capturing infinite-dimensional memory effects.

To ensure the feasibility and reliability of our study, we employed a systematic approach grounded in discrete fractional calculus. The fractional-order APD map was derived analytically using the Caputo-like delta operator, following established definitions and theorems in discrete fractional dynamics. Numerical simulations were conducted using high-precision computation in MATLAB, with stepwise variation of the stimulation period t_s and controlled initial conditions. The dynamical behavior of the system was examined using three complementary methods: bifurcation diagrams, to detect qualitative transitions such as period-doubling and chaotic windows, Lyapunov exponent plots, to quantify sensitivity to initial conditions and detect chaos and 0–1 test for chaos, which offers a modern, non-traditional diagnostic tool to confirm chaoticity using only time series data. The convergence among these methods strengthens the validity of our findings. Parameters were taken directly from Lewis and Guevara's model [23] to ensure biological relevance, and the fractional order was chosen based on a balance between memory influence and computational feasibility.

The proposed fractional discrete model offers several potential practical applications in both theoretical and clinical contexts. In particular, its ability to capture long-memory effects in cardiac action potential dynamics makes it well-suited for modeling arrhythmias such as alternans and ventricular fibrillation, which are strongly influenced by past cardiac cycles. This could inform the design of improved diagnostic tools or pacing strategies that account for memory in cardiac tissues. Furthermore, the model may serve as a computational framework for simulating drug effects on cardiac electrophysiology, especially when the drug-induced modifications exhibit delayed or cumulative behavior. The discrete-time formulation also makes it computationally efficient and easily integrable into larger-scale simulations of cardiac tissue or whole-heart models.

We begin our study by recalling some essential definitions from discrete fractional calculus.

2. Discrete-time fractional calculus

This section delves into the essential definitions that form the foundation of discrete fractional calculus, a fascinating area of study that blends traditional calculus with discrete mathematical concepts.

Let $a \in \mathbb{R}$ and let $\mathbb{N}_a$ denote the set of all discrete numbers starting from a, ie, $\mathbb{N}_a = \{a, a+1, a+2, \dots\}$. For a function $u(n)$, the delta difference operator Δ is defined as

$$\Delta u(n) = u(n+1) - u(n). \tag{2.1}$$

Definition 2.1. [5] Let $u : \mathbb{N}_a \to \mathbb{R}$ and $\varrho > 0$. Then the fractional sum of ϱ order

is defined by

$$\Delta_a^{-\varrho} u(t) = \frac{1}{\Gamma(\varrho)} \sum_{s=a}^{t-\varrho} (t - \sigma(s))^{(\varrho-1)} u(s), \ t \in \mathbb{N}_{a+\varrho}, \tag{2.2}$$

where a is the starting point, $\sigma(s) = s+1$ and $t^{(\varrho)}$ is the falling function defined in terms of the gamma function as

$$t^{(\varrho)} = \frac{\Gamma(t+1)}{\Gamma(t+1-\varrho)}. \tag{2.3}$$

Definition 2.2. [3] For $\varrho > 0$, $\varrho \notin \mathbb{N}$ and $u(t)$ defined on $\mathbb{N}_a$, the Caputo-like delta difference is defined in the following manner:

$$\begin{aligned} {}^c\Delta_a^{\varrho} u(t) &= \Delta_a^{-(m-\varrho)} \Delta^m u(t) \\ &= \frac{1}{\Gamma(m-\varrho)} \sum_{s=a}^{t-(m-\varrho)} (t - \sigma(s))^{(m-\varrho-1)} \Delta_s^m u(s), \end{aligned} \tag{2.4}$$

where $t \in \mathbb{N}_{a+m-\varrho}$, $m = [\varrho] + 1$.

The subsequent theorem provides a basis for defining the numerical formula for the proposed system.

Theorem 2.1. *[10] For the delta fractional Caputo-like discrete initial value problem*

$$\begin{cases} {}^c\Delta_a^{\varrho} u(t) = f(t+\varrho-1, u(t+\varrho-1)), \\ \\ \Delta^k u(t) = u_k \text{ for } k = 0, 1, \ldots, m-1 \text{ where } \ m = [\varrho] + 1, \end{cases} \tag{2.5}$$

the equivalent discrete integral equation can be obtained as

$$u(t) = u_0(t) + \frac{1}{\Gamma(\varrho)} \sum_{s=a+m-\varrho}^{t-\varrho} (t-\sigma(s))^{(\varrho-1)} f(s+\varrho-1, u(s+\varrho-1)), \ t \in \mathbb{N}_{a+m}, \tag{2.6}$$

where

$$u_0(t) = \sum_{k=0}^{m-1} \frac{(t-a)^{(k)}}{k!} \Delta^k u(a). \tag{2.7}$$

The existence results for the nonlinear fractional difference equation discussed in [9] have been presented. Specifically, if the initial point $a = 0$ and $0 < \varrho < 1$, then equation (2.6) can be rewritten as follows:

$$u(t) = u(0) + \frac{1}{\Gamma(\varrho)} \sum_{s=1-\varrho}^{t-\varrho} (t - \sigma(s))^{(v-1)} f(s+\varrho-1, u(s+\varrho-1)), \ t \in \mathbb{N}_m. \tag{2.8}$$

Using $(t-\sigma(s))^{(\varrho-1)} = \frac{\Gamma(t-s)}{\Gamma(t-s+\varrho+1)}$, and $s+\varrho = j$, equation (2.8) is further simplified to

$$u(t) = u(0) + \frac{1}{\Gamma(\varrho)} \sum_{j=1}^{t} \frac{\Gamma(t-j+\varrho)}{\Gamma(t-j+1)} f(j-1, u(j-1)). \tag{2.9}$$

3. One-dimensional cardiac action potential duration mapping model without memory

Lewis and Guevara [23] undertook a detailed simulation aimed at examining the effects of periodic stimulation on a strand of ventricular muscle. This investigation was meticulously conducted through the numerical integration of the one-dimensional cable equation, yielding significant insights into the mechanisms of cardiac physiology. They considered the equation that reads

$$(a/2R_j)\partial^2 V/\partial x^2 = C\partial V/\partial t + I_m, \tag{3.1}$$

where the Beeler-Reuter model is employed to accurately represent transmembrane currents. This enabled them to simplify the analysis of a partial differential equation, which is typically infinite dimensional, down to a one-dimensional map. Additionally, this approach demonstrated that concepts from non-linear dynamics—such as bifurcations with period doubling, bi-stability, and chaotic behavior—can effectively explain the phenomena observed in the numerical simulations of the cable equation.

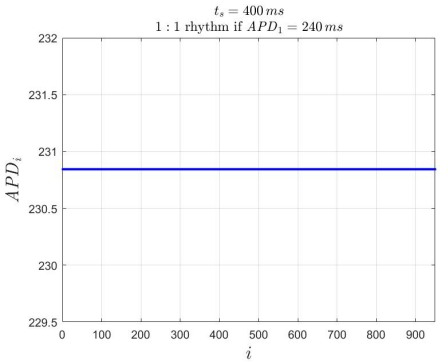

(a)

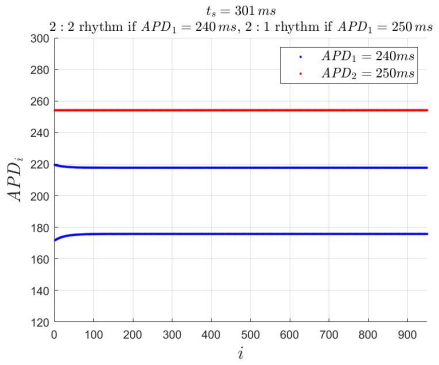

(b)

Figure 1. (a) Iterates asymptotically converge to the stable period-1 orbit, corresponding to a $1:1$ rhythm. (b) Bi-stability: Iterates converge to the stable period-1 orbit, corresponding to a $2:1$ rhythm for $APD_1 = 250ms$ and to a period-2 orbite, corresponding to a $2:2$ rhythm for $APD_1 = 240ms$

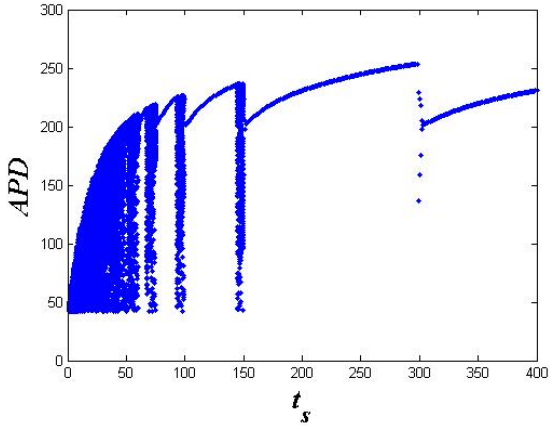

Figure 2. Bifurcation diagram of map (3.2) (APD vs t_s)

We first consider a simple one-dimensional map that lacks memory. This iterative system of the action potential duration (APD) is proposed in [23] as

$$x_{i+1} = f(x_i),\ i \in \mathbb{N},$$

or

$$x_{i+1} = A - B_1 \exp\left(\frac{x_i - nt_s}{\tau_1}\right) - B_2 \exp\left(\frac{x_i - nt_s}{\tau_2}\right). \tag{3.2}$$

$x_i \in [0, 270\ msec]$, where x_{i+1} is the APD generated by the $(i+1)$th stimulus and let n the parameter block in the production of an action potential on the condition that $(nt_s - x_{i+1} \geq DI_{\min})$. The constants: $A, B_1, B_2, \tau_1, \tau_2, DI_{\min}$ are related to the cardiac electro-physiological constraints of the heart defined by Lewis and Guevara [23]:

$$\begin{aligned} &A = 270\ msec,\ \ B_1 = 2441\ msec,\ B_2 = 90.02\ msec, \\ &\tau_1 = 19.6\ msec,\ \tau_2 = 200.5\ msec,\ DI_{min} = 53.5\ msec. \end{aligned} \tag{3.3}$$

Note that an $N : M$ rhythm ($N \geq 1$, $M \geq 1$) is periodic with period Nt_s, consisting of repeating $N : M$ cycles, each containing N stimulus pulses, and M action potentials with distinct morphologies.

Figures 1(a) and 1(b) show plots of APD_i $vs.$ i for various t_s. Figure 1(a) ($t_s = 400\ msec$) demonstrates that the trajectory of map (3.2) converges to a stable steady-state or period-1 orbit, $APD_i = APD_{i+1} = 231\ msec$ in an alternating manner (the period-1 orbit is asymptotically stable). This steady-state corresponds to a $1 : 1$ rhythm with an $APD = 231\ msec$. This period-1 orbit remains stable until $t_s = 301.8\ msec$, where it becomes unstable and is replaced by a period-2 orbit, corresponding to a $2 : 2$ rhythm. This period-2 orbit arises out of a period-doubling bifurcation. This happens if an initial condition $APD_1 < 248\ msec$. However if the initial condition$APD_1 > 248\ msec$ the iterates converge to a period-1 orbit at $APD_i = APD_{i+1} = 254\ msec$, corresponding to a $2 : 1$ rhythm Figure 1(b). Bi-stability is thus present on the map (iterates converge to one orbit or the other depending upon the initial condition).

Figure 2 shows a bifurcation diagram (APD vs. t_s) which summarizes the changes in steady-state dynamics of the map (3.2). We note that as the frequency of the stimulation in the Figure 2 is increased, the frequency of bifurcation of the rhythms for any initial condition $APD_1 \leq 248$ $msec$ is given by frequency $= \{1 : 1 \longrightarrow 2 : 1 \longrightarrow 4 : 2 \longrightarrow chaos \longrightarrow 3 : 1 \longrightarrow 6 : 2 \longrightarrow chaos \longrightarrow 4 : 1 \longrightarrow 8 : 2 \longrightarrow chaos \longrightarrow 5 : 1 \longrightarrow 10 : 2 \longrightarrow chaos \longrightarrow 6 : 1 \longrightarrow total\ chaos\}$, and for any initial condition $APD_1 \geq 248$ $msec$ the frequency of bifurcation of the rhythms is given by frequency $= \{1 : 1 \longrightarrow 2 : 2 \longrightarrow 2 : 1 \longrightarrow 4 : 2 \longrightarrow chaos \longrightarrow 3 : 1 \longrightarrow 6 : 2 \longrightarrow chaos \longrightarrow 4 : 1 \longrightarrow 8 : 2 \longrightarrow chaos \longrightarrow 5 : 1 \longrightarrow 10 : 2 \longrightarrow chaos \longrightarrow 6 : 1 \longrightarrow total\ chaos\}$.

In equation (3.2), APD_n relies solely on its immediately preceding value, APD_{n-1}, indicating that it does not account for any memory effects. However, cardiac systems do exhibit memory, where the action potential duration (APD) depends not only on the most recent value but also on earlier APDs. To capture this memory effect, a higher-dimensional iterated map is necessary. As illustrated in reference [21], the authors employed a two-dimensional map to explore the nonlinear dynamics arising from memory effects as follows:

$$x_{i+1} = A - B_1 exp\left(\frac{(x_i/a) - nt_s}{\tau_1}\right) - B_2 exp\left(\frac{(x_{i-1}/a) - nt_s}{\tau_2}\right), \tag{3.4}$$

where a denotes a positive real parameter. The model incorporates a degree of memory, as it connects the duration of the next action potential, represented by x_{i+1}, to the two preceding action potential durations, x_i and x_{i-1}.

In this study, we present a model of cardiac action potential duration (APD) that exhibits long memory. Specifically, the current state of the system is influenced by all previous states. To accomplish this, we utilize the Caputo fractional order difference operator. The decision to adopt a long memory model is grounded in the observation that excitable systems, including chaotic systems, possess memory. This memory can lead to dynamic instabilities in excitation, as well as chaos [22].

4. The fractional order APD map

The first order difference (3.2) can be reformulated as

$$\triangle x(i) = A - B_1 \exp\left(\frac{x(i) - nt_s}{\tau_1}\right) - B_2 \exp\left(\frac{x(i) - nt_s}{\tau_2}\right) - x(i). \tag{4.1}$$

The application of the Caputo-like delta operator ${}^c\Delta_a^{\varrho}$, with a designated as the starting point, to equation (4.1) yields a novel fractional order cardiac action potential duration (APD) map that reads

$$\begin{aligned} {}^c\Delta_a^{\varrho} x(t) =& A - B_1 exp\left(\frac{x(t+\varrho-1) - nt_s}{\tau_1}\right) - B_2 exp\left(\frac{x(t+\varrho-1)) - nt_s}{\tau_2}\right) \\ & - x(t+\varrho-1). \end{aligned} \tag{4.2}$$

According to Theorem 2.1, taking the initial point as 0, the solution of equation (4.2) takes the form

$$x_i = x_0 + \frac{1}{\Gamma(\varrho)} \sum_{j=1}^{i} \frac{\Gamma(i-j+\varrho)}{\Gamma(i-j+1)} \left(A - B_1 exp\left(\frac{x_{j-1} - nt_s}{\tau_1}\right)\right.$$

$$-B_2 exp\left(\frac{x_{j-1} - nt_s}{\tau_2}\right) - x_{j-1}\Bigg), \tag{4.3}$$

where $0 < \varrho < 1$ is the fractional order of discrete dynamical system (4.3).

Comparing maps (3.2) with (3.4), the fractional order map (4.3) exhibits a long memory effect. This means that the current state of evolution x_i is influenced by all previous states $x_0, x_1, \ldots, x_{i-1}$.

Before we begin our numerical investigation, it is important to note that, similar to fractional-order continuous-time systems, fractional-order discrete systems cannot support non-constant periodic solutions. Consequently, the fractional-order system described by equation (4.3) does not allow for periodic orbits [13]. However, it is essential to recognize that this system may possess numerical periodic orbits (NPOs), where the trajectories might approximate periodic solutions.

4.1. Dynamics of the fractional order APD

This subsection aims to explore both the regular and chaotic behaviors of the fractional discrete map (4.3) using numerical simulations for the parameter set (3.3).

We strategically select fractional order ϱ, which signifies the memory effect, to maintain a balance between dynamic richness and proximity to the integer case $\varrho = 1$. After extensive testing, we confidently settle on $\varrho = 0.92$.

This study explores the impact of systematically decreasing the stimulation frequency t_s from 400 $msec$ to 40 $msec$ by increments of 0.1. Initiating from the baseline condition $APD_1 = 200$ $msec$, we successfully generated the bifurcation diagram presented in Figure 3(a).

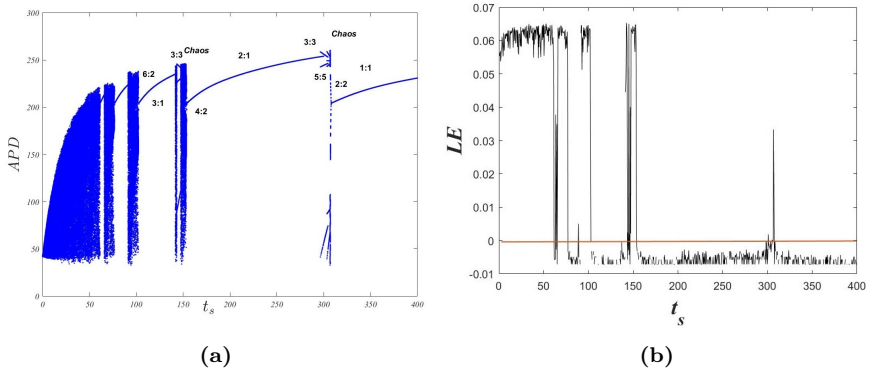

(a) **(b)**

Figure 3. (a) Bifurcation diagram in the (ϱ,APD) plan for $\varrho = 0.92$, $APD_1 = 200$ $msec$ and t_s varying from 0 to 400, (b) Lyapunov exponents corresponding to the bifurcation diagram

By analyzing the bifurcation diagram we see that for $t_s = 400$ $msec$ the stable steady-state or period 1 orbit at $APD_n = APD_{n+1} = 230.8$ $msec$ is asymptotically approached. This steady state corresponds to a $1:1$ normal rhythm. As t_s is decreased, the period 1 orbit becomes unstable and is replaced by a stable period-2 NPO corresponding to a $2:2$ rhythm or alternans. This period-2 NPO arises out from a period doubling bifurcation that occurs at $t_s = 308$ $msec$ Figure 4(a). As t_s is decreased still further, the period-2 NPO grows in amplitude until at $t_s = 307$ $msec$. It disappears in an abrupt fashion and is replaced by an irregular

rhythm. It is crucial to acknowledge that alternans frequently occur as a precursor to malignant ventricular arrhythmias. These can be indicative of an early phase in a period-doubling cascade, which may ultimately progress to chaotic dynamics associated with ventricular fibrillation. A thorough understanding of this relationship is valuable for effective monitoring and management of potential cardiac risks. In our case and unlike what it was observed in the integer order system, the chaos appears suddenly, not being preceded by any period-doubling bifurcation.

When we reduce the parameter t_s until the value 307 $msec$ we observe the formation of a period-5 NPO which corresponds to a $5:5$ rhythm which lasts up to $t_s = 304.9$ $msec$, value for which a period-3 NPO corresponding to a $3:3$ rhythm appears. The $3:3$ and $5:5$ rhythms will alternate along the interval $303.2\ msec \leq t_s \leq 304.9\ msec$ as we see in Figure 4(b), where we note that the length of the interval of the $3:3$ rhythm increases while that of the $5:5$ rhythm decreases until it disappears at $ts = 303.2$ $msec$, and only the $3:3$ rhythm remains. By decreasing t_s, the same scenario will be repeated in the interval $296.4\ msec \leq t_s \leq 300.1\ msec$ but with an alternation between $3:3$ and $2:1$ rhythms, see Figure 4(c).

As t_s is decreased still further, one observes a period doubling bifurcation at $t_s = 154$ $msec$ and the $2:1$ rhythm is replaced by a $4:2$ rhythm, after what an irregular rhythm is produced at the values of t_s lying between 142.1 $msec$ and 153.6 $msec$. In this chaotic interval, we can see a period-3 window for $143.4\ msec \leq ts \leq 146.9\ msec$. As t_s is reduced in the range $142.1\ msec > t_s \geq 40\ msec$ in 0.1 $msec$ steps, one repeatedly sees transitions of the form $\{n:1 \to 2n:2 \to irregular \to n+1:1\}$ with $3 \leq n \leq 5$.

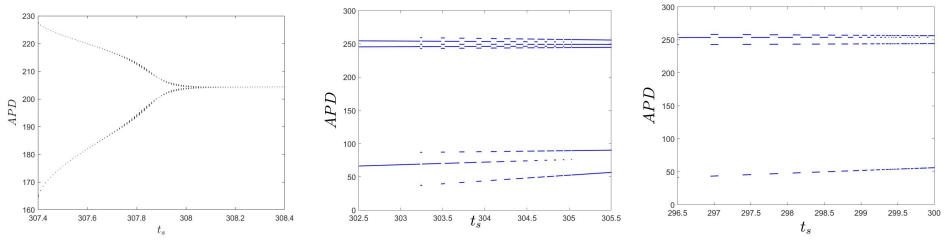

(a) **(b)** **(c)**

Figure 4. Expanded view of bifurcation diagram: (a) appearance of $2:2$ rhythm (alternans) at $t_s = 308$ $msec$, (b) in range $t_s = 303.2 - 304.9$ $msec$ we can see alternation between $5:5$ and $3:3$ rhythms, (c) in range $t_s = 296.4 - 300.1$ $msec$ alternation between $2:1$ and $3:3$ rhythms

Thus, for the initial condition $APD_1 = 200$ $msec$, we can summarize the dynamics of the system by the following sequence

$$\begin{aligned} sequence = \{&1:1 \to 2:2 \to chaos \to 5:5 \xrightarrow{\text{altenation}} 3:3 \xrightarrow{\text{altenation}} 2:1 \to 4:2 \\ &\to chaos \to 3:3 \to chaos \to 3:1 \to 6:2 \to chaos \to 4:1 \to 8:2 \\ &\to chaos \to 5:1 \to 10:2 \to chaos\}. \end{aligned}$$

For an initial condition $APD_1 = 250$ $msec$, one obtains the bifurcation diagram in Figure 5(a). We notice the absence of alternans (2:2 rhythm), and chaos appears abruptly in a border collision bifurcation, so we have the following sequence

bifurcation:

$$\begin{aligned} sequence = \{1:1 \to chaos \to 5:5 \xrightarrow{\text{altenation}} 3:3 \xrightarrow{\text{altenation}} 2:1 \to 4:2 \to chaos \\ \to 3:3 \to 3:1 \to 6:2 \to chaos \to 4:1 \to 8:2 \\ \to chaos \to 5:1 \to 10:2 \to chaos\}. \end{aligned}$$

Bistability is a significant characteristic of the fractional order map APD. The iterates decisively converge to one orbit or the other based on the selected initial condition, APD_1:

- the bistability $\{2:2 \leftrightarrow chaos\}$ at $t_s = 307.5\ msec$,
- the bistability $\{5:5 \leftrightarrow 3:3\}$ at $t_s = 305\ msec$,
- the bistability $\{3:3 \leftrightarrow 2:1\}$ at $t_s = 300\ msec$,
- the bistability $\{chaos \leftrightarrow 3:1\}$ at $t_s = 143\ msec$.

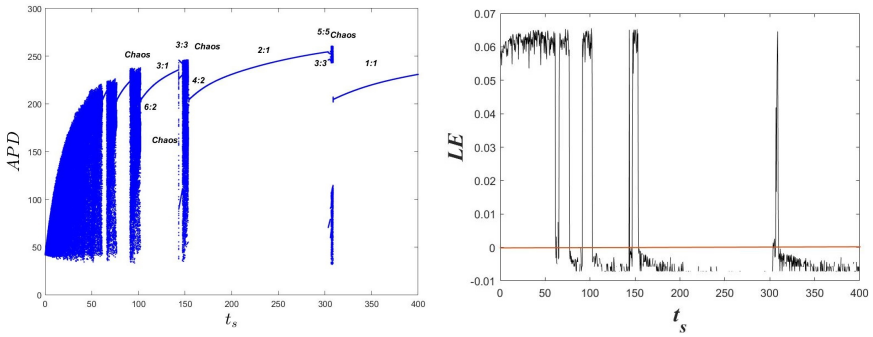

(a) **(b)**

Figure 5. (a) Bifurcation diagram in the (t_s,APD) plan for $\varrho = 0.92$, $APD_1 = 250\ msec$ and t_s varynig from 0 to 400, (b) Lyapunov exponents corresponding to the bifurcation diagram

4.2. Chaos in the fractional order APD

This section investigates the chaotic behavior of the fractional discrete map (4.3) through numerical simulations with the parameters specified in (3.3). We employ two powerful tools for analyzing chaos: Lyapunov exponents and the 0-1 test. The Lyapunov exponent (LE) is an important metric in chaos theory that evaluates the sensitivity of a system to small changes in initial conditions. It provides a quantitative measure of the rate at which trajectories that start close together diverge from each other, thereby offering valuable insights into the system's chaotic behavior. A positive Lyapunov exponent indicates that nearby initial points will exponentially diverge over time, suggesting chaotic behavior. On the other hand, a negative Lyapunov exponent signifies stability in a dynamical system, ensuring that nearby trajectories will remain closely aligned. The definition of the Lyapunov exponent is as follows:

$$\lambda = \lim_{n\to\infty} \frac{1}{n} \sum_{i=0}^{n-1} \ln |f'(x_i)|$$

where $f(x_i)$ is time series generated by chaotic system and n is the size of time series.

The lyapunov exponents for system (4.3) are shown in Figure 3(b) for $APD_1 = 200\ msec$ and Figure 5(b) for $APD_1 = 250\ msec$. They are in perfect agreement with the corresponding bifurcation diagrams.

The 0-1 test, developed in [16], is a method used to determine whether a given sequence exhibits chaotic behavior. The input for the test is time-series data, while the output is either 1, indicating chaotic behavior similar to Brownian motion, or 0, signifying non-chaotic behavior where the motion remains bounded [25]. For $c \in [0, \pi]$, we calculate the test result K of a sequence $\phi(j)$, where $j = 1, 2, \ldots, n$, as follows:

$$K = \lim_{n\to\infty} \frac{\log M_c(n)}{\log n},$$

where $M_c(n)$ is the mean square displacement defined as

$$M_c(n) = \lim_{N\to\infty} \sum_{j=1}^{N} [p_c(j+n) - p_c(j)]^2 + [q_c(j+n) - q_c(j)]^2.$$

Here $p_c(n)$ and $q_c(n)$ are the translation variables defined as:

$$p_c(n) = \sum_{j=1}^{n} \phi(j)\cos(jc) \qquad q_c(n) = \sum_{j=1}^{n} \phi(j)\sin(jc).$$

We now embark on applying the 0-1 test to the discrete series data APD_n for $\varrho = 0.92$, with $APD_1 = 200\ msec$ and various values of t_s derived from the parameter set defined in (3.3).

Table 1 and Figure 6 showcase the results of this important test for different t_s values. Notably, for $t_s = 100\ msec$ and $t_s = 152\ msec$, the asymptotic growth rates K of the fractional order map reveal remarkable values: $K = 0.9960$ and $K = 0.9870$, respectively.

The unbounded behavior of the translation component within the $p - q$ plane, as vividly depicted in Figures 6(a) and 6(b), showcases a series of Brownian-like trajectories that suggest a rich tapestry of chaotic dynamics. These captivating results harmonize beautifully with the bifurcation and Lyapunov exponent diagrams illustrated in Figure 3, painting a comprehensive picture of the system's behavior. In stark contrast, when we examine the values of $t_s = 80\ msec$ and $t_s = 250\ msec$, the 0–1 test nears zero, leading to the emergence of bounded trajectories, as highlighted in Figures 6(c) and 6(d). This transition confirms that the fractional-order map transforms into a periodic motion for these specific time intervals, offering profound insights into the underlying order amid apparent chaos.

t_s (msec)	80	100	152	250
K	0.0113	0.9960	0.9870	0.0540

Table 1. Results of the 0–1 test for the fractional-order APD map, showing that as $K \to 1$ the dynamics are chaotic, and as $K \to 0$ the dynamics are periodic.

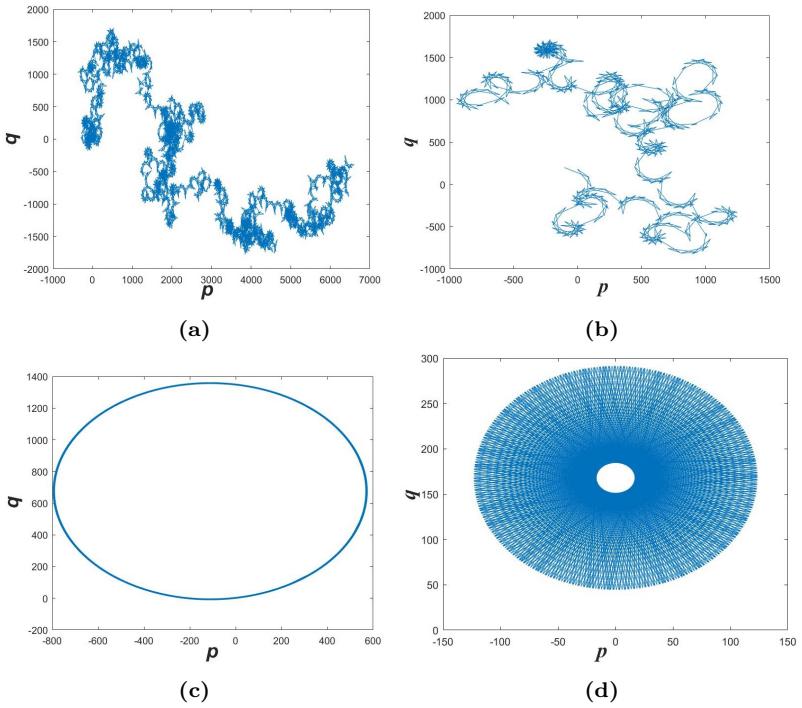

Figure 6. The 0-1 test of the fractional-order discrete system (4.3): (a) for $t_s = 100\ msec$, (b) $t_s = 152\ msec$ (c) $t_s = 80\ msec$ and (d) $t_s = 250\ msec$

5. Conclusion and discussion

This work introduced a novel fractional-order one-dimensional map for the cardiac action potential duration (APD), extending the traditional model by incorporating long-memory dynamics through the Caputo-like delta operator. By doing so, we have revealed complex and rich nonlinear dynamics that are qualitatively different from those observed in the memoryless and short-memory APD maps.

The results demonstrate that the fractional-order map captures a broader range of cardiac dynamics, including the early onset of chaos, the absence of alternation in certain conditions, and new bistability patterns (e.g., $\{2:2 \longleftrightarrow chaos\}$, $\{5:5 \longleftrightarrow 3:3\}$), which have not been reported in prior literature. The combined use of bifurcation analysis, Lyapunov exponents, and the 0–1 test confirms the reliability of these observations and provides a robust framework for characterizing complex cardiac dynamics.

These findings highlight the significance of long memory in cardiac dynamics, providing deeper insights into the initiation and evolution of arrhythmias. The proposed model offers a foundation for exploring new anti-arrhythmic treatments and paves the way for more accurate patient-specific modeling.

Future studies can build upon this work by focusing on the control and synchronization of chaotic dynamics in the proposed fractional-order cardiac model. In particular, applying advanced control theory techniques will enable the design of targeted strategies to suppress undesirable arrhythmic behavior, stabilizing the dynamics towards healthy cardiac rhythms. Moreover, exploring synchronization

methods can shed light on how cardiac tissue achieves coherent activity, opening new avenues for the prevention and treatment of arrhythmias through coupling and phase synchronization approaches.

References

[1] A. Abbes, A. Ouannas, A. Hioual and S. Momani, *Hidden chaos in a new memristor-based discrete system with commensurate, incommensurate and variable fractional orders*, Physica Scripta, 2024, 99(10), 105233.

[2] A. Abbes, A. Ouannas, N. Shawagfeh and H. Jahanshahi, *The fractional-order discrete covid-19 pandemic model: stability and chaos*, Nonlinear Dyn., 2023, 111, 965–983.

[3] T. Abdeljawad, *On Riemann and Caputo fractional differences*, Comp. Math. Appl., 2011, 62(3), 1602–1611.

[4] O. A. Almatroud and V. T. Pham, *Building fixed point-free maps with memristor*, Mathematics, 2023, 11(6), 1319.

[5] F. Atici and P. Eloe, *Initial value problems in discrete fractional calculus*, Proc. Am. Math. Soc, 2009, 137(3), 981–989.

[6] R. Bououden and M. S. Abdelouahab, *Chaotic optimization algorithm based on the modified probability density function of lozi map*, Boletim da Sociedade Paranaense de Matematica, 2021, 39(6), 9–22.

[7] R. Bououden, M. S. Abdelouahab, F. Jarad and Z. Hammouch, *A novel fractional piecewise linear map: Regular and chaotic dynamics*, International Journal of General Systems, 2021, 50(5), 501–26.

[8] S. I. Bouzeraa, R. Bououden and M. S. Abdelouahab, *Fractional logistic map with fixed memory length*, International Journal oh General Systems, 2023, 52(6), 653–663.

[9] F. Chen, X. Luo and Y. Zhou, *Existence results for nonlinear fractional difference equation*, Adv. Differ. Equ., 2011, (713201).

[10] F. Chen, X. Luo and Y. Zhou, *Existence results for nonlinear fractional difference equations*, Adv. Differ. Eqs., 2011, 713201.

[11] D. Dai, X. Li, Z. Li et al., *Numerical simulation of the fractional-order Lorenz chaotic systems with Caputo fractional derivative*, Comput. Model. Eng. Sci., 2023, 135(2), 1371–1392.

[12] B. V. der Pol and J. van der Mark, *The heartbeat considered as a relaxation oscillation, and an electrical model of the heart*, Philosophical Magazine and Journal of Science, 1928, 6(38), 763–775.

[13] J. Diblik, M. Feckan and M. Pospísíl, *Nonexistence of periodic solutions and s-asymptotically periodic solutions in fractional difference equations*, Appl. Math. Comput., 2015, 257, 230–240.

[14] V. Elharrar and B. Surawicz, *Cycle length effect on restitution of action potential duration in dog cardiac fibers*, Am. J. Physiol. Heart Circ. Physiol., 1983, 244(6), H782–92.

[15] J. Fox, M. Riccio, P. Drury et al., *Dynamic mechanism for conduction block in heart tissue*, New J. Phys., 2003, 5(1), 101.

[16] G. Gottwald and I. Melbourne, *A new test for chaos in deterministic systems*, P. R. Soc. A Math. Phys. Sci., 2004, 460(2042), 603–611.

[17] T. Hamadneh, A. A. H. Al-Tarawneh, G. M. Gharib et al., *On chaos and complexity analysis for a new sine-based memristor map with commensurate and incommensurate fractional orders*, Mathematics, 2023, 11(20), 4308.

[18] T. Houmor, H. Zerimeche and A. Berkane, *Dynamical behaviors of fractional-order Selkov model and its discretization*, Nonlinear Dynamics and Systems Theory, 2021, 21(3), 246–261.

[19] C. Ionescu, A. Lopes, D. Copot et al., *The role of fractional calculus in modeling biological phenomena: A review*, Communications in Nonlinear Science and Numerical Simulation, 2017, 51, 141–159.

[20] H. Karagueuzian, H. Stepanyan and W. Mandel, *Bifurcation theory and cardiac arrhythmias*, Am. J. Cardiovasc. Dis., 2013, 3(1), 1–16.

[21] M. Kesmia, S. Boughaba and S. Jacquir, *Nonlinear dynamics of two-dimensional cardiac action potential duration mapping model with memory*, J. Math. Biol., 2019, 8(5), 1529–1552.

[22] J. Landaw, A. Garfinkel, J. N. Weiss and Z. Qu, *Memory-induced chaos in cardiac excitation*, Phys. Rev. Lett., 2017, 118(13), 407–432.

[23] T. Lewis and M. Guevara, *Chaotic dynamics in a ionic model of the propagated cardiac action potential*, Theor. Biol, 1990, 146(3), 407–432.

[24] W. Mobitz, *Über die unvollstandige störung der erregungsüberleitung zwischen vorhof und kammer des menschlichen herzens*, Z. Ges. Exp. Med, 1924, 41, 180–237.

[25] M. Nicol, I. Melbourne and P. Ashwin, *Euclidean extensions of dynamical systems*, Nonlinearity, 2001, 14(2), 275–300.

[26] J. Nolasco and R. Dahlen, *A graphic method for the study of alternation in cardiac action potentials*, J. Appl. Physiol, 1968, 25(2), 191–196.

[27] Z. Qu, Y. Shiferaw and J. N. Weiss, *Nonlinear dynamics of cardiac excitation-contraction coupling: an iterated map study*, Phys. Rev. E., 2007, 75(1), 011927.

[28] F. Rihan, *Numerical modeling of fractional-order biological systems*, Abstract and Applied Anaysis, 2013, 2013(816803,), 1–11.

[29] R. B. Robinson, P. A. Boyden, B. F. Hoffman and K. Hewett, *Electrical restitution process in dispersed canine cardiac purkinje and ventricular cells.*, Am. J. Physiol. Heart Circ. Physiol., 1987, 253(5 Pt 2), H1018–25.

[30] R. Saadeh, A. Abbes, A. Al-Husban et al., *The fractional discrete predator-prey model: chaos, control and synchronizations*, Fractal Fract., 2023, 7(2), 7020120.

[31] N. Sene, *Introduction to the fractional-order chaotic system under fractional operator in Caputo senses*, Alex. Eng. J., 2021, 60(4), 3997–4014.

[32] F. E. Serrano, J. M. Munoz-Pacheco and M. A. Flores, *Fractional-order projection of a chaotic system with hidden attractors and its passivity-based synchronization*, Front. Appl. Math. Stat., 2023, 60, 1267664.

[33] E. Tolkacheva, M. M. Romeo, M. Guerraty and D. J. Gauthier, *Condition for alternans and its control in a two-dimensional mapping model of paced cardiac dynamics*, Phys. Rev. E, 2004, 69(3), 031904.

[34] E. G. Tolkacheva, D. G. Schaeffer, D. J. Gauthier and W. Krassowska, *Condition for alternans and stability of the 1: 1 response pattern in a memory model of paced cardiac dynamics*, Phys. Rev. E, 2003, 67(3), 31904.

[35] H. Zerimeche, T. Houmor and A. Berkane, *Combination synchronization of different dimensions fractional-order non-autonomous chaotic systems using scaling matrix*, International Journal of Dynamics and Control, 2021, 9, 788–796.